applied optics

Measurement of back-scattering patterns from single laser trapped aerosol particles in air

Yong-Le Pan,[1,*] Chuji Wang,[2] Leonid A. Beresnev,[1] Alex J. Yuffa,[1] Gorden Videen,[1] David Ligon,[1] and Joshua L. Santarpia[3]

[1]Army Research Laboratory, 2800 Powder Mill Road, Adelphi, Maryland 20783, USA
[2]Department of Physics and Astronomy, Mississippi State University, Starkville, Mississippi 39759, USA
[3]Sandia National Laboratories, Albuquerque, New Mexico 87123, USA
*Corresponding author: yongle.pan.civ@mail.mil

Received 22 July 2016; revised 4 August 2016; accepted 5 August 2016; posted 10 August 2016 (Doc. ID 272251); published 20 September 2016

We demonstrate a method for measuring elastic back-scattering patterns from single laser trapped micron-sized particles, spanning the scattering angle range of $\theta = 167.7°$–$180°$ and $\phi = 0°$–$360°$ in spherical coordinates. We calibrated the apparatus by capturing light-scattering patterns of 10 μm diameter borosilicate glass microspheres and comparing their scattered intensities with Lorenz–Mie theory. Back-scattering patterns are also presented from a single trapped Johnson grass spore, two attached Johnson grass spores, and a cluster of Johnson grass spores. The method has potential use in characterizing airborne aerosol particles, and may be used to provide back-scattering data for lidar applications.

OCIS codes: (010.1350) Backscattering; (120.5820) Scattering measurements; (010.1100) Aerosol detection; (140.7010) Laser trapping; (010.1310) Atmospheric scattering; (280.1310) Atmospheric scattering.

http://dx.doi.org/10.1364/AO.56.0000B1

1. INTRODUCTION

Elastic light scattering is sensitive to aerosol size, shape, surface roughness, and chemical properties. It is considered to have the potential to be a means of continuous real-time *in situ* detection and differentiation of aerosol particles, even potentially life-threatening bioaerosols from normal atmospheric background constituents [1–8]. Increases in computational capabilities and improved theoretical algorithms have made it possible to calculate the light scattering from highly irregular heterogeneous systems [9–15]. There remains a demand for experimental data that can be used for verification of both exact theory and approximations used in such calculations. The principal resource for such data has been the light-scattering facilities currently located in Granada [16] that have provided the gold-standard data used for such comparisons. Unfortunately, these data are obtained for distributions of particles. There also is a need for single-particle data that can be used for direct theoretical comparisons. While some data from naturally occurring particles have been obtained in the past (e.g., Refs. [3,4,6,17]), these instruments obtained scattering patterns from single particles by designing a flow-through system that triggers when a particle enters a measurement area (e.g., Refs. [1–6,8]). Another possibility is to trap single particles for detailed measurements, such as the pioneering works done in measuring the angular distribution of the scattering intensity from a single trapped biological cell in liquid [18,19], or to obtain particle size information from a trapped airborne droplet [20,21] using laser tweezers. A stable trap allows the time-resolved dynamic measurements of particle properties. Our instrument is designed to further address this need for light-scattering information from single airborne solid particles. In this work, we focus on the back-scattering region. Whereas, the forward-scattering region is determined largely by diffraction and is sensitive to particle morphology, the back-scattering region is sensitive especially to particle heterogeneities and surface structure, including roughness [22]. A recent report of the measured scattered light distribution in the range of polar scattering angle-theta from $180° \pm 6°$ showed the extreme sensitivity of the back-scattering to particle parameters [23]. One unique aspect of our instrument is that it can measure the two-dimensional light-scattering signal in the region centered on the exact back-scattering angle ($\theta = 180°$), covering the range of $\theta = 167.7°$–$180°$, and $\phi = 0°$–$360°$ in spherical coordinates without any moving parts. It is not trivial to obtain the scattering signals from a single micron-size particle at the exact back-scattering angle at $\theta = 180°$ since stray scattered light from optical components is significant. Recently developed technology makes it possible to stably trap both transparent and absorbing solid particles in air using one laser beam configuration [24] and allows us to make this measurement.

In this paper, we demonstrate a method that can be used to measure the elastic back-scattering pattern from a single

micron-sized particle trapped in air. Here, we trap both transparent and absorbing particles with arbitrary morphology with a single shaped laser beam [24]. The back-scattered intensity patterns are $I(\theta, \phi)$ captured in the angular range of $\theta = 167.7°$–$180°$, $\phi = 0°$–$360°$ from these particles and recorded on a CCD. Here, θ is the polar angle relative to the z axis that is defined by the direction of the incident laser beam, and ϕ is the azimuthal angle relative to some arbitrarily determined x axis, in this case, perpendicular to the laboratory floor.

2. EXPERIMENTAL SETUP

A schematic of the experimental arrangement with the corresponding coordinates is shown in Fig. 1. All tested aerosol particles are commercially purchased dry particles that are introduced into the trapping cell by sprinkling them using a cotton tipped swab through a hole in the top of the enclosed cell. The cell is used to minimize the perturbations caused by air flow in the lab. This hole is an adjustable iris that can be closed when particles are delivered into the cell. A power-adjustable 532 nm laser (up to 3 W) is used to trap the particles. It is spatially filtered (L4, PH2, L5), and then formed into a collimated hollow beam after passing two axicons (AL1, AL2). The hollow beam is reflected vertically upward by a reflective mirror (M), and then focused by an aspheric lens (ASL1: numerical aperture, N.A. = 0.60; effective focal length, efl = 12 mm) to create an upward hollow optical cone with a focal point at the vertex. Particles are trapped in air at or near the focal point depending on the particle properties [24]. The trapped particle is illuminated by a circularly polarized 465 nm laser beam propagating horizontally (defined to be along the z axis). This beam is spatially filtered and collimated (L1, PH1, L2) before passing through a polarizing beam splitter (PBS1) and a quarter-wave plate ($\lambda/4$ WP) to circularly polarize the incident beam. It is lightly focused (L3) before being reflected by a nonpolarized beam splitter (BS) toward the trapped particle. The back-scattered light is transmitted through the same BS, and then passes through the collecting lens ASL2 (efl = 50 mm). The light then passes through a linearly polarizing analyzer (LPA) and a short pass filter (SP) before reaching the CCD detector (CCD1) that records the scattering pattern. The collecting lens ASL2 is aligned so that the trapped particle is in the back focal point of the lens. A ray emerging from the focal point and entering the lens at an angle θ and emerging parallel to the optical axis of the lens with an off-axis displacement r satisfies the Abbe sine condition as $r = f \sin\theta$. Through the sine condition, the x and y coordinates of the recorded pattern on the camera CCD1 are traced back to the scattering angles θ, ϕ as shown in the inset of Fig. 1. As polarimetric techniques supply more information about aerosols in an elastic scattering pattern and in Lidar systems (e.g., Refs. [7,11,25,26]), we have recorded thousands of vertically and horizontally polarized scattering patterns by aligning the LPA in the two directions; a detailed analysis of the polarimetric results will be presented in the near future.

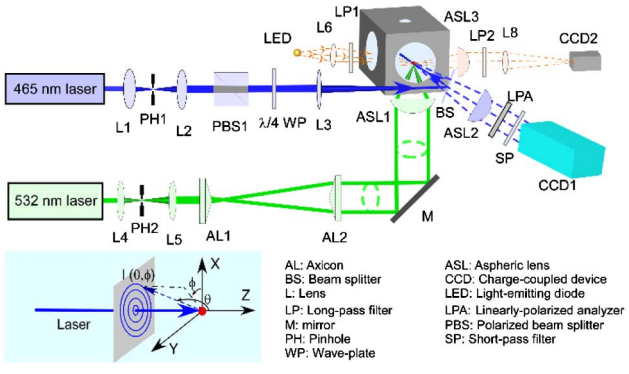

Fig. 1. Experimental setup for measuring elastic back-scattering patterns from single trapped aerosol particles. The inset shows the coordinate system, and the legend of acronyms is in the lower right.

3. RESULTS AND DISCUSSIONS

Figure 2 shows two sets of typical back-scattering patterns recorded by CCD1 (the upper and middle rows) from different trapped particles whose images are shown in the bottom row, which is the light-emitting diode (LED) illuminated shadow images recorded by CCD2. Patterns in set 1 and set 2 were obtained through repeated measurements from the same trapped particle with a time separation of ~10 min. From the left to the right in each set, the trapped particles are a single glass sphere (Duke Scientific 9010, ~10 μm), a single Johnson grass spore (~8 μm, Greer, P1285045), two attached Johnson grass spores with the longer dimension oriented approximately in the vertical direction, and a cluster of Johnson grass spores (~14 μm). As the borosilicate glass microsphere has weak absorption at 532 nm, it is trapped in air mainly by the radiation pressure force. The laser power used for the trapping was 1.4 W. Johnson grass has strong absorption in visible light, and it is trapped mainly by the photophoretic force. The laser power used for the trapping was 100 mW. Once a particle is captured, it can be trapped stably in air and may even be kept in the same orientation for hours using a much lower trapping laser power. In addition, the 465 nm illumination laser used for generating the light-scattering patterns also contributes to the photophoretic and radiation pressure forces for the

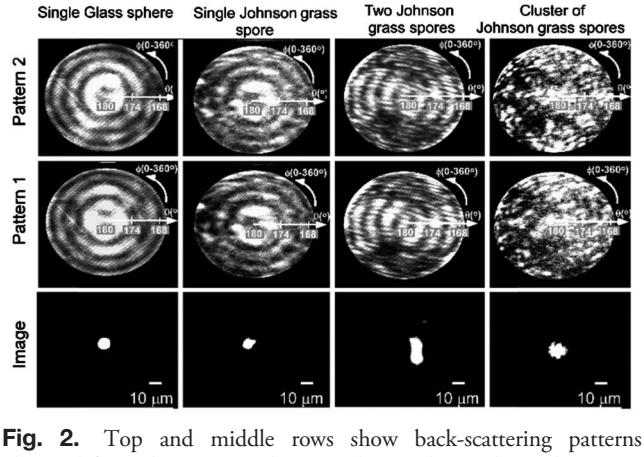

Fig. 2. Top and middle rows show back-scattering patterns obtained from the same single trapped aerosol particles with 10 min time separation in the two measurements. The bottom row shows an image of the trapped aerosol particle. The images of each column are for different particle types.

trapping. Consequently, the trapping position is slightly different when the illuminating laser is operating. In order to keep all trapped particles located in the same position, which should be within a few microns of each other so that their scattering signals can be captured by CCD1, the 465 nm illuminating laser was kept as low as 18 mW after the BS. The positions and shapes of the trapped particles are monitored by CCD2 either through illumination by a white LED or the 465 nm laser.

Once a particle is trapped, barring significant disturbance, it can remain trapped for hours. In some cases, a trapped particle oscillates around a point with a displacement of up to tens of microns or may rotate around an axis. We present results from some stably trapped particles. A comparison of the patterns in sets 1 and 2 of Fig. 2 from the same trapped particle shows that patterns obtained over 10 min intervals can be very similar. For nonspherical particles, this means that the particle must not have moved or rotated significantly during this period. Although there is no noticeable movement or rotation for the stable trapped particles observed from the images during the pattern recording period, the scattering pattern still presented some subtle variations that may be caused by a very fine rotation or movement of the trapped particle, such as the two patterns from the cluster of Johnson grass spores for ϕ around 220°–320° in column 4. This demonstrates that this technique could be much more sensitive to monitoring the fine change of a studied particle (e.g., orientation, size) than the direct image method. It should be sensitive enough to observe small changes in particle morphology, and may be suitable for monitoring changes under different atmospheric conditions, including humidity, ozone concentration, etc.

Glass microspheres have reasonably smooth surfaces and a homogeneous density distribution. In the forward-scattering region, their light scattering is governed largely by diffraction and is expected to appear as concentric rings. Diffraction is nonexistent in the back-scattering region, where we expect to see greater dependence on asymmetries, heterogeneities, and surface roughness. The patterns from the sphere in Fig. 2 (first column) display concentric rings with some minor intensity variations. The Johnson grass spore (second column) has a rough surface and sphere-like shape. Its pattern still displays a ring structure similar to a microsphere but containing more perturbations. The pattern from two attached spores still bear a strong resemblance to those of the single sphere, but with the addition of an interference pattern due to the two scattering centers. Such patterns have been examined in the past for spheres [13,14,27]. We also note the horizontal band of strong intensity that has been noted for such agglomerate particles. We realize that the spatial frequency in the vertical direction is approximately twice that of the horizontal direction, which is as we would expect from a particle whose extent is half as great in this direction. The scattering patterns in the last column are obtained from a trapped cluster of Johnson grass spores whose total diameter is ~14 μm. The patterns show the typical scattering structures from clusters formed by a group of smaller particles [5,27].

NIST traceable borosilicate glass microspheres (Duke Scientific 9010, diameter $d = 10.0\ \mu\text{m} \pm 1.0\ \mu\text{m}$, index of refraction $n = 1.56$ at 589 nm, 23°C [28]) were used to test and calibrate the apparatus. Figure 3 shows a comparison of the experimental measurement with Lorenz–Mie simulations [29] from a single trapped glass sphere. The Lorenz–Mie simulation was obtained using a microsphere with a refractive index $n = 1.567 + i0$, and radii of $r = 5.050$; 5.055; 5.0625; 5.065; and 5.070 μm, where n is obtained from Refs. [28,30] and $r = 5.0625$ μm is found to be the best fit by comparing the Lorenz–Mie simulations with the measured data. The experimental data used for the scattering intensity curve were averaged over all angles ϕ. For a perfect microsphere, the scattering intensity in different ϕ at a given θ should be the same under the illumination of a circularly polarized laser. However, variations in the ring intensity indicate that the trapped sphere and the polarization's circularity are not perfect. This also explains the minor discrepancy between the experimental and the theoretical data for the intensity distribution along the scattering angle θ. The Lorenz–Mie calculation also shows that the back-scattering glory at 180° from a spherical particle do not necessarily appear at all sizes. Even with a change of 0.1% in size [$r = 5.050$ μm to 5.055 μm; for a few nanometer (nm) radii difference], the scattering intensity can change from a minimum to a maximum at 180°. We note that such sensitivity of the back-scattering intensity is also seen for other particle parameters, including the refractive index [23]. Such results are relevant in assessing aerosol metrology using lidar.

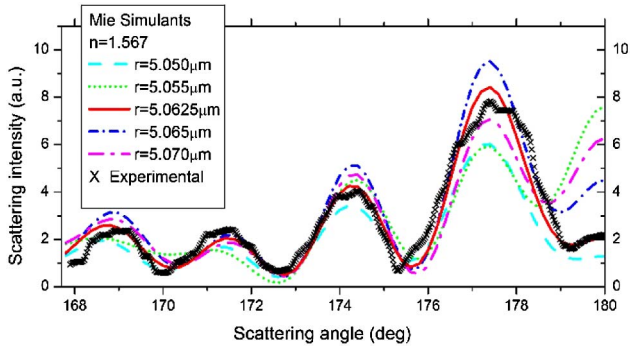

Fig. 3. Angle (θ) dependence of back-scattering intensities of a single glass microsphere optically trapped in air. The plot shows the comparison between experimental measurements (black symbol ×) and Lorenz–Mie calculations (lines).

4. SUMMARY

In this paper, we have demonstrated that we can stably trap aerosol particles for long periods of time and measure their light scattering over the backward hemisphere, isolating the scattering signal from stray light. The light-scattering patterns are reproducible over minutes to hours, suggesting that even the particle orientation is stable. Using this new method combined with other spectroscopic techniques (e.g., Raman and laser induced fluorescence spectroscopy), one should be able to study time- and particle-resolved physical and chemical properties of bioaerosol, chemical aerosol, and atmospheric aerosol without inference from chemical and environmental matrixes or under particularly controlled environmental conditions

(temporal effect of relative humidity, ozone concentration, oxidation, contamination, etc.). A database of individual particle scattering may offer information for potential particle classification and differentiation.

Funding. Defense Threat Reduction Agency (DTRA) (HDTRS1518237, HDTRA1619734); U.S. Army Research Laboratory (ARL).

REFERENCES

1. P. J. Wyatt, "Identification of bacteria by differential light scattering," Nature **221**, 1257–1258 (1969).
2. M. Bartholdi, G. C. Salzman, R. D. Hiebert, and M. Kerker, "Differential light scattering photometer for rapid analysis of single particles in flow," Appl. Opt. **19**, 1573–1581 (1980).
3. P. H. Kaye, K. Alexander-Buckley, E. Hirst, and S. Saunders, "A real-time monitoring system for airborne particle shape and size analysis," J. Geophys. Res. **101**, 19215–19221 (1996).
4. R. A. West, L. R. Doose, A. M. Eibl, M. G. Tomasko, and M. I. Mishchenko, "Laboratory measurements of mineral dust scattering phase function and linear polarization," J. Geophys. Res. **102**, 16871–16881 (1997).
5. Y.-L. Pan, K. B. Aptowicz, R. K. Chang, M. Hart, and J. D. Eversole, "Characterizing and monitoring respiratory aerosols by light scattering," Opt. Lett. **28**, 589–591 (2003).
6. K. B. Aptowicz, R. G. Pinnick, S. C. Hill, Y.-L. Pan, and R. K. Chang, "Optical scattering patterns from single urban aerosol particles at Adelphi, Maryland, USA: a classification relating to particle morphologies," J. Geophys. Res. **111**, D12212 (2006).
7. X. Cao, G. Roy, and R. Bernier, "Lidar polarization discrimination of bioaerosols," Opt. Eng. **49**, 116201 (2010).
8. Y.-L. Pan, M. J. Berg, S. S. M. Zhang, H. Noh, H. Cao, R. K. Chang, and G. Videen, "Measurement and autocorrelation analysis of two-dimensional light-scattering patterns from living cells for label-free classification," Cytometry A **79**, 284–292 (2011).
9. M. I. Mishchenko, L. D. Travis, and A. A. Lacis, *Scattering, Absorption, and Emission of Light by Small Particles* (Cambridge University, 2002).
10. C. M. Sorensen and D. Shi, "Patterns in the ripple structure of Mie scattering," J. Opt. Soc. Am. A **19**, 122–125 (2002).
11. E. Zubko, Y. Shkuratov, M. Hart, J. Eversole, and G. Videen, "Backscattering and negative polarization of agglomerate particles," Opt. Lett. **28**, 1504–1506 (2003).
12. M. J. Berg, C. M. Sorensen, and A. Chakrabarti, "Explanation of the patterns in Mie theory," J. Quant. Spectrosc. Radiat. Transfer **111**, 782–794 (2010).
13. G. Videen, W. Sun, Q. Fu, D. R. Secker, R. Greenaway, P. H. Kaye, E. Hirst, and D. Bartley, "Light scattering from deformed droplets and droplets with inclusions: II. Theoretical treatment," Appl. Opt. **39**, 5031–5039 (2000).
14. D. R. Secker, R. Greenaway, P. H. Kaye, E. Hirst, D. Bartley, and G. Videen, "Light scattering from deformed droplets and droplets with inclusions: I. Experimental results," Appl. Opt. **39**, 5023–5030 (2000).
15. G. Videen, W. Sun, and Q. Fu, "Light scattering from irregular tetrahedral aggregates," Opt. Commun. **156**, 5–9 (1998).
16. O. Muñoz, F. Moreno, D. Guirado, D. D. Dabrowska, H. Volten, and J. W. Hovenier, "The Amsterdam–Granada light scattering database," J. Quant. Spectrosc. Radiat. Transfer **113**, 565–574 (2012).
17. K. B. Aptowicz, Y.-L. Pan, S. D. Martin, E. Fernandez, R. K. Chang, and R. G. Pinnick, "Decomposition of atmospheric aerosol phase function by particle size and asphericity from measurements of single particle optical scattering patterns," J. Quant. Spectrosc. Radiat. Transfer **131**, 13–23 (2013).
18. R. M. P. Doornbos, M. Schaeffer, A. G. Hoekstra, P. M. A. Sloot, B. G. de Grooth, and J. Greve, "Elastic backscattering measurements of single biological cells in an optical trap," Appl. Opt. **35**, 729–734 (1996).
19. D. Watson, N. Hagen, J. Diver, P. Marchand, and M. Chachisvilis, "Elastic light scattering from single cells: orientational dynamics in optical trap," Biophys. J. **87**, 1298–1306 (2004).
20. M. D. Barnes, N. Lermer, W. B. Whitten, and J. M. Ramsey, "A CCD based approach to high-precision size and refractive index determination of levitated microdroplets using Fraunhofer diffraction," Rev. Sci. Instrum. **68**, 2287–2291 (1997).
21. M. Guillon, K. Dholakia, and D. McGloin, "Optical trapping and spectral analysis of aerosols with a supercontiuum laser source," Opt. Express **16**, 7655–7664 (2008).
22. G. E. Fernandes, Y.-L. Pan, R. K. Chang, K. Aptowicz, and R. G. Pinnick, "Simultaneous forward- and backward-hemisphere elastic-light-scattering patterns of respirable-size aerosols," Opt. Lett. **31**, 3034–3036 (2006).
23. B. M. Heffernan, Y. W. Heinson, J. B. Maughan, A. Chakrabarti, and C. M. Sorensen, "Backscattering measurements of micron-sized spherical particles," Appl. Opt. **55**, 3214–3218 (2016).
24. B. Redding and Y.-L. Pan, "Optical trap for both transparent and absorbing particles in air using a single shaped laser beam," Opt. Lett. **40**, 2798–2801 (2015).
25. M. Hayman and J. P. Thayer, "General description of polarization in lidar using Stokes vectors and polar decomposition of Mueller matrices," J. Opt. Soc. Am. A **29**, 400–409 (2012).
26. J. M. Sanz, P. Albella, F. Moreno, J. M. Saiz, and F. González, "Application of the polar decomposition to light scattering particle systems," J. Quant. Spectrosc. Radiat. Transfer **110**, 1369–1374 (2009).
27. S. Holler, J. C. Auger, B. Stout, Y.-L. Pan, J. R. Bottiger, R. C. Chang, and G. Videen, "Observations and calculations of light scattering from cluster of spheres," Appl. Opt. **39**, 6873–6887 (2000).
28. Distrilab Particle Technology, "9000 series—glass size beads," http://www.distrilabparticles.com/products/nist-traceable-particle-size-standards/9000-series-glass-size-beads/.
29. P. Laven, "MiePlot: a computer program for scattering of light from a sphere using Mie theory and the Debye series," http://www.philiplaven.com/mieplot.htm.
30. M. Polyanskiy, "Refractive index database," http://refractiveindex.info/?shelf=glass&book=HIKARI-BK&page=J-BK7A.